www.czasopisma.pan.pl PAN www.journals.pan.pl
Chemical and Process Engineering 2018, 39 (2), 143–154
DOI: 10.24425/119105

THREE-DIMENSIONAL COMPUTATIONAL FLUID DYNAMICS MODELLING OF A PROTON EXCHANGE MEMBRANE FUEL CELL WITH A SERPENTINE MICRO-CHANNEL DESIGN

Tomasz Zinko*, Paulina Pianko-Oprych, Zdzisław Jaworski

West Pomeranian University of Technology, Szczecin, Faculty of Chemical Technology and Engineering, Institute of Chemical Engineering and Environmental Protection Processes, al. Piastów 42, 71-065 Szczecin, Poland

The aim of this paper was to demonstrate the feasibility of using a Computational Fluid Dynamics tool for the design of a novel Proton Exchange Membrane Fuel Cell and to investigate the performance of serpentine micro-channel flow fields. A three-dimensional steady state model consisting of momentum, heat, species and charge conservation equations in combination with electrochemical equations has been developed. The design of the PEMFC involved electrolyte membrane, anode and cathode catalyst layers, anode and cathode gas diffusion layers, two collectors and serpentine micro-channels of air and fuel. The distributions of mass fraction, temperature, pressure drop and gas flows through the PEMFC were studied. The current density was predicted in a wide scope of voltage. The current density – voltage curve and power characteristic of the analysed PEMFC design were obtained. A validation study showed that the developed model was able to assess the PEMFC performance.

Keywords: Proton Exchange Membrane Fuel Cells, Computational Fluid Dynamics, flow field design, polarisation curve

1. INTRODUCTION

Fuel cells are attractive and promising power generation devices due to their high power density and low pollutant emissions. Compared to conventional chemical combustion systems which are currently most common, a key benefit of fuel cell is theoretically high-energy efficiency (Li et al., 2010). From a few kinds of fuel cells, Proton Exchange Membrane Fuel Cell (PEMFC) is characterised by low operating temperature (less than 100 °C) which makes it quick to start up and easy to handle (Kunusch et al., 2012). The complexity of the phenomena that are involved inside a PEMFC, despite a huge number of performed studies and experiments, results in still active areas of necessary research including reduction of cost, weight and size of cells as well as increase of durability and performance. Fuel cells are sensitive to changes of operation conditions and also susceptible to potential damage.

One of the crucial aspects is the level of oxygen in PEMFC (Vega-Leal et al., 2007). In the case of too low amount of oxidizer, undesirable hot spots appear in the membrane and output power decreases, which is called cathode/ oxygen starvation. On the other hand, too high oxygen flow affects its ionic resistance and implies on higher power demand for supplying air, reducing the overall system performance. The application of a new design solution of a cathode parallel flow-field with a three sub-channel inlets allowed to improve the fuel cell performance (Yue L. et al., 2017). As a result, the maximum power density increased

* Corresponding author, e-mail: tomasz.zinko@zut.edu.pl

by more than 13.2% compared to a conventional design. The opposite conclusion was formulated by Taymaz and Kahveci (2018), who claimed that increasing oxygen flow rate did not cause a significant change in the performance, contrary to the humidification and cell temperature.

Another issue is proper membrane water content, which has critical impact on the protonic conductivity, water transport properties, mechanical resistance and gas permeability (Kunusch et al., 2012). Several mechanisms determine the amount of water present: water permeability as a result of pressure difference between anode and cathode channels, diffusion due to the water concentration gradient across the membrane, water generation on the cathode side at a rate proportional to the electric current produced and electro-osmotic drag induced by water molecules dragged by the proton flow from anode to cathode. Understanding water transport mechanism is crucial for estimating the performance and durability of fuel cells. Moreover, the results of study conducted by Taner (2018) indicated that control over water production affected significantly the fuel cell life-time. It was concluded that a small-scale PEMFC could be modelled for enhancement of fuel cells. PEMFC performance could be improved by optimising the parameters like pressure, flow rate and voltage.

Numerical modelling can improve fundamental understanding of the mechanisms and reactions that take place within fuel cells. Distribution of reactants over the surface of electrodes is vital for an optimal operation of PEMFC. One of the first models of PEMFC was based on empirical relationships that do not consider gas dynamics (Springer et al., 1991). It was a one-dimensional and steady-state model. Moreover, a three-dimensional, single-phase, isothermal model was applied with fully humidified gas feed and validated against the current distribution data (Ju and Wang, 2004). A comparison of simulations and experiments pointed out a lack of agreement in the current distribution despite the average polarisation curves which matched nearly perfectly. Water behaviour in the air-water flow inside a U-shaped microchannel for PEMFC was studied (Quan et al., 2005). It has been proved that the bend area of a serpentine flow channel has significant effects on the flow field and water flooding could occur in the "after-bend" section. This may block the reactant supply to reaction sites which decreases fuel cell performance. Furthermore, the sub-rib convection, which was affected by the serpentine flow field, significantly influenced the cell performance when the oxygen supply or membrane moisture content was limited (Wang et al., 2009). It was shown that changing channel aspect ratio had a slight effect on cell performance but the oxygen supply was sufficient for a single serpentine flow field. The gas-liquid flow in micro-channels and transport layer of PEMFC was analysed numerically with a VOF model by Lafmejani et al. (2017). Due to the complexity of phenomena, the effect of electrochemistry has to be considered as negligible. It was observed that the wall film thickness changes due to the difference in phase superficial velocities from the bottom to the top of the outgoing channel from 0 to 200 μm. The electrochemical reactions were taken into consideration in order to obtain liquid water saturation in PEMFC and to simulate the air-water two-phase flow in the cathode gas channel by Ferreira et al. (2017).

The presented work describes the results of numerical performance investigation for a PEMFC novel design distinguished by serpentine micro-channel flow fields. In order to obtain voltage-current characteristics of the PEMFC, a three-dimensional model was developed in the Computational Fluid Dynamics (CFD) commercial software ANSYS Fluent 15.0 with an additional Fuel Cell Tools module (ANSYS Inc., 2015). The steady-state simulations considered momentum, species, mass and heat transfer as well as the transport of electric current driven by electric potential in combination with electrochemical reactions.

2. PHYSICAL AND NUMERICAL MODEL

Fuel cell converts chemical energy of fuels into electric energy. The process can be described by the fundamental reaction (1), which usually happens in three steps enabled by catalysts (2)–(4). Ions are transported from one reaction site to the other inside the fuel cell. In the meantime, electrons have to

pass through the external electrical circuit because of a semipermeable membrane. This generates usable voltage (power).

$$H_2 + \frac{1}{2}O_2 \rightarrow H_2O \tag{1}$$

$$H_2 \rightarrow 2H^+ + 2e^- \tag{2}$$

$$\frac{1}{2}O_2 + 2e^- \rightarrow O^{2-} \tag{3}$$

$$2H^+ + O^{2-} \rightarrow H_2O \tag{4}$$

Fuel cell consists of the anode, cathode and membrane. In the case of a Proton Exchange Membrane Fuel Cell (PEMFC), the membrane is a proton conducting polymer material. Catalyst layers on both sides of the membrane and touching it, also called electrodes, are porous mediums which allow diffusive flow of gases (fuel on anode side and air on cathode one) and electron transport. Gas diffusion layers (GDL) are also porous environments which permit diffusive flow (in void regions) and electron transport (in solid regions). Gas channels supply fuel and oxidiser on the anode and cathode sides, respectively, and exhaust reaction products and untapped substrates. Current collectors are solid materials used to conduct electrons to the external electrical circuit and provide structural stability. All functional regions are shown in Fig. 2.

During modelling of the PEMFC fluid flow with reacting species, heat and mass transfer, electrochemical heterogeneous reactions, transport of electric current driven by electric potential and phase change in the case of occurrence of liquid water were considered. Therefore, fuel cell operation was governed by the mass, momentum, species and energy conservation Eqs. (5)–(8), respectively:

$$\nabla \cdot (\rho \bar{v}) = 0 \tag{5}$$

$$\nabla \cdot (\rho \bar{v}\bar{v}) = -\nabla p + \nabla(\mu \nabla \bar{v}) + S_M \tag{6}$$

$$\nabla \cdot (\rho \bar{v} y_j) = \nabla \cdot (\rho D_j \nabla y_j) + S_j \tag{7}$$

$$\nabla \cdot (\rho c_p T \bar{v}) = \nabla \cdot \left((\varepsilon k_f + (1-\varepsilon) k_s) \nabla T - \sum_j c_p T J_j \right) + S_h \tag{8}$$

The momentum source term, S_M, was defined by Eq. (9) in the gas diffusion layers and the catalyst layers. In other zones it was equal to zero.

$$S_M = -\frac{\mu}{K}\varepsilon \bar{v} \tag{9}$$

The volumetric energy source term, S_h, was described by Eq. (10), where $I^2 R_{\text{ohm}}$ was the ohmic heating term and ηR was the electric work term.

$$S_h = I^2 R_{ohm} + h_{\text{reaction}} + \eta R_{an,cat} + h_{\text{phase}} \tag{10}$$

The heterogeneous reactions that take place on the catalyst surfaces were accompanied by the rate of species production as described in Eq. (11).

$$\frac{\rho D_j}{\delta}\left(y_{j,surf.f} - y_{j,cent}\right) \cdot r = \frac{M_{w,j}}{nF} R_{an,cat} \tag{11}$$

The gas phase species diffusivity was calculated according to Eq. (12).

$$D_j = \varepsilon^{1.5} \cdot (1-s)^{r_s} \cdot D_j^0 \left(\frac{p^0}{p}\right)\left(\frac{T}{T^0}\right)^{1.5} \tag{12}$$

The species source terms of Eq. (7), S_j, were defined in Eq. (13)–(15) for fluid zones and were zero for others.

$$S_{\mathrm{H_2}} = -\frac{M_{w,\mathrm{H_2}}}{2F} R_{an} \tag{13}$$

$$S_{\mathrm{O_2}} = -\frac{M_{w,\mathrm{O_2}}}{4F} R_{cat} \tag{14}$$

$$S_{\mathrm{H_2O}} = \frac{M_{w,\mathrm{H_2O}}}{2F} R_{an} \tag{15}$$

Electron transport through the solid conducting regions including the catalyst layer, the porous electrode (GDL) and the current collectors as well as proton conductivity through the electrolyte were calculated with Eqs. (16) and (17), respectively.

$$\nabla \cdot (\sigma_s \nabla \varphi_s) + R_s = 0 \tag{16}$$

$$\nabla \cdot (\sigma_m \nabla \varphi_m) + R_m = 0 \tag{17}$$

The membrane electrical conductivity was calculated by an empirical formula (18). The volumetric transfer current was defined according to the Butler-Volmer equation as shown in Eqs. (19)–(20).

$$\sigma_m = \beta \varepsilon (0.514\lambda - 0.26)^{\varpi} e^{1268\left(\frac{1}{303} - \frac{1}{T}\right)} \tag{18}$$

$$R_{an} = j_{an}^{ref} \left(\frac{X_{\mathrm{H_2}}}{X_{\mathrm{H_2}}^{ref}} \right)^{\gamma_{an}} \left(e^{\alpha_{an} F \eta_{an}/RT} - e^{-\alpha_{cat} F \eta_{an}/RT} \right) \tag{19}$$

$$R_{cat} = j_{cat}^{ref} \left(\frac{X_{\mathrm{O_2}}}{X_{\mathrm{O_2}}^{ref}} \right)^{\gamma_{cat}} \left(-e^{\alpha_{an} F \eta_{cat}/RT} + e^{-\alpha_{an} F \eta_{cat}/RT} \right) \tag{20}$$

The activation loss, η, was calculated as the difference between the solid and membrane potentials as shown in Eqs. (21)–(22), where V_{OC} was the open circuit voltage.

$$\eta_{an} = \varphi_s - \varphi_m \tag{21}$$

$$\eta_{cat} = \varphi_s - \varphi_m - V_{OC} \tag{22}$$

In this study a novel design of Proton Exchange Membrane Fuel Cell with a serpentine micro-channels flow fields was used in CFD calculations. The PEMFC geometry with gas distribution and dimensions is presented in Fig. 1, while functional regions with boundary conditions for the electric and protonic

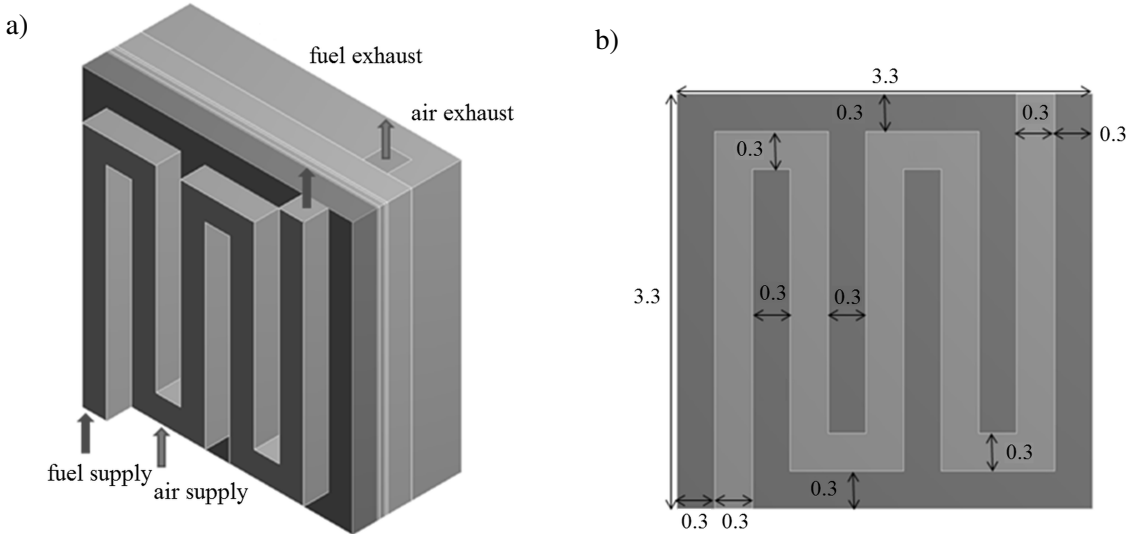

Fig. 1. PEMFC geometry: a) gas distribution, b) dimensions [mm]

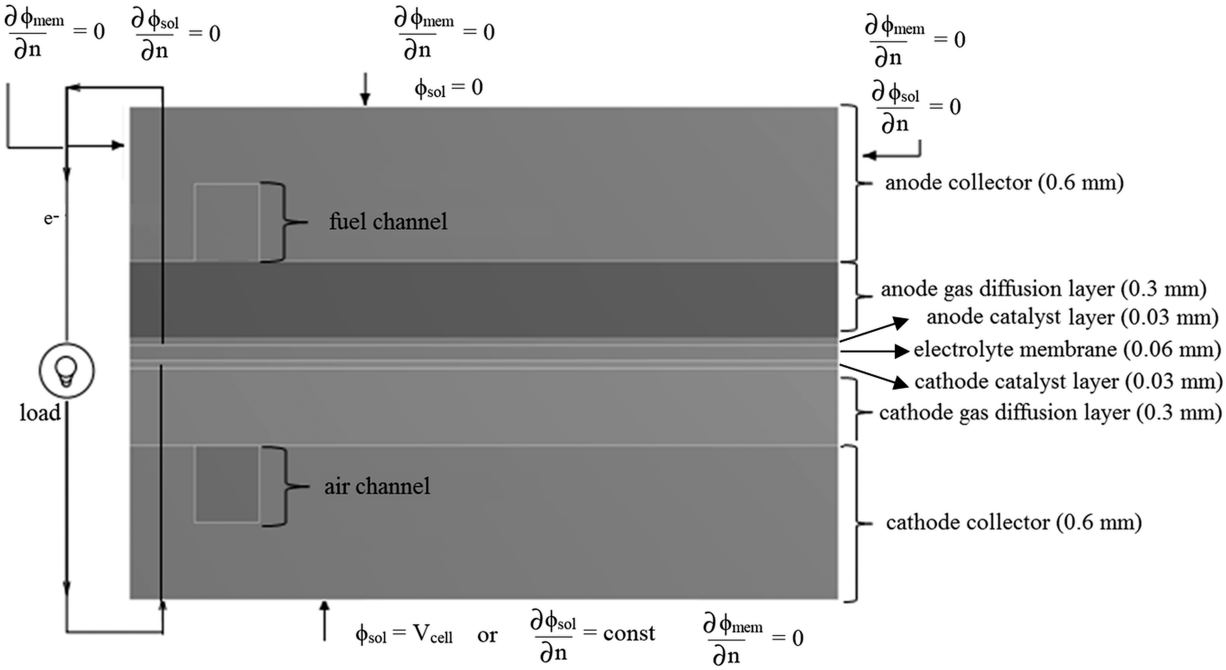

Fig. 2. Boundary conditions and regions of the PEMFC

Table 1. Material properties

Component	Property	Value	Unit
Current collector	Density	2719	kg/m^3
	Specific heat capacity	871	J/(kg·K)
	Thermal conductivity	100	W/(m·K)
	Electrical conductivity	1×10^6	1/(Ohm·m)
Catalyst layer/ Gas diffusion layer	Density	2719	kg/m^3
	Specific heat capacity	871	J/(kg·K)
	Thermal conductivity	10	W/(m·K)
	Electrical conductivity	5000	1/(Ohm·m)
Electrolyte	Density	1980	kg/m^3
	Specific heat capacity	2000	J/(kg·K)
	Thermal conductivity	2	W/(m·K)
	Electrical conductivity	1×10^{-16}	1/(Ohm·m)

potential fields are shown in Fig. 2. Material properties and operating parameters are summarised in Table 1 and Table 2, respectively.

In Fig. 3, the applied mesh consisting of 51 thousand hexahedral cells is presented. During simulations the current density was obtained in a wide scope of voltage from 1.05 V to 0.3 V with a step of 0.15 V. In ad-

dition, the following assumptions were used in the developed approach: steady-state operating conditions, incompressible and laminar flow since the velocity of the gases was low, ideal gas mixtures, all material parameters were isotropic and homogenous, all electrochemical reactions were gaseous phase reactions, isothermal operation.

Table 2. Physical and operating parameters used in the model

Model parameter	Value	Unit
Thickness of current collector	0.6	mm
Depth of flow channels in collectors	0.3	mm
Thickness of anode/ cathode gas diffusion layer	0.3	mm
Thickness of anode/ cathode catalyst layer	0.03	mm
Thickness of electrolyte	0.06	mm
Operating temperature	80 (353)	°C (K)
Inlet/outlet fuel/air temperature	80 (353)	°C (K)
Inlet mass flow rate of fuel	6×10^{-7}	kg/s
Inlet species of fuel (mass ratio) H_2:H_2O	0.8:0.2	–
Inlet mass flow rate of air	5×10^{-6}	kg/s
Inlet species of air (mass ratio) O_2:H_2O:N_2	0.2:0.1:0.7	–
Outlet fuel/air pressure	200000	Pa
Voltage at anode terminal surface	0	V
Voltage at cathode terminal surface	0.3–1.05	V
Open Circuit Voltage (OCV)	1.1	V
Anode ref. current density	10000	$A \cdot m^2$
Anode ref. concentration	1	$kmol/m^3$
Anode concentration exponent	0.5	–
Anode exchange coefficient	2	–
Cathode ref. current density	20	$A \cdot m^2$
Cathode ref. concentration	1	$kmol/m^3$
Cathode concentration exponent	1	–
Cathode exchange coefficient	2	–
Reference diffusivity	3×10^{-5}	–
Viscous resistance of porous zone	1E12	$1/m^2$
Catalyst layer, anode & cathode porosity	0.5	–
Electrolyte equivalent weight	1100	kg/kmol
Electrolyte protonic conduction coefficient	1	–
Electrolyte protonic conduction exponent	1	–

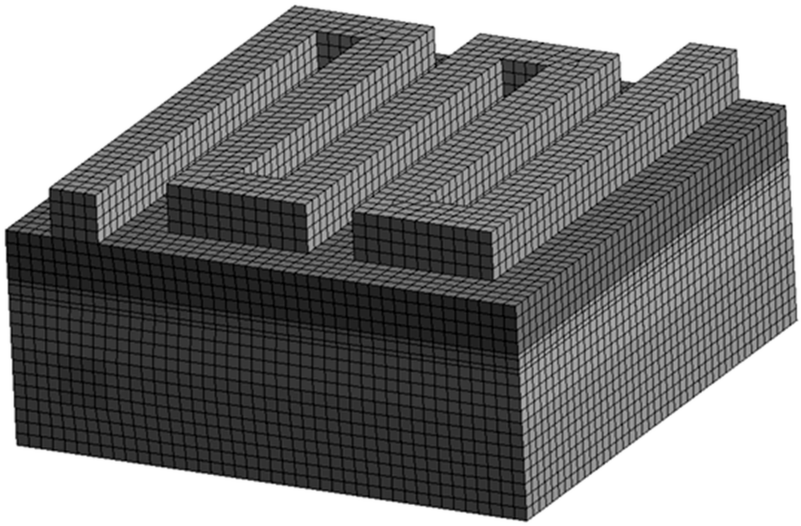

Fig. 3. PEMFC mesh

3. RESULTS AND DISCUSSION

The calculated polarisation curve and power density characteristic in a wide scope of voltage from 1.05 V to 0.3 V are presented in Fig. 4 for a novel design of Proton Exchange Membrane Fuel Cell with a serpentine micro-channel flow fields. For the design of the PEMFC the greatest power was observed in the voltage range between 0.6 and 0.45 V. The CFD current-voltage characteristic has not been compared with measurement data as the literature lacks results for the new conceptual geometry design of the planar fuel cell in smaller scale. The current scope of this work was to carry out only numerical calculations without building a prototype.

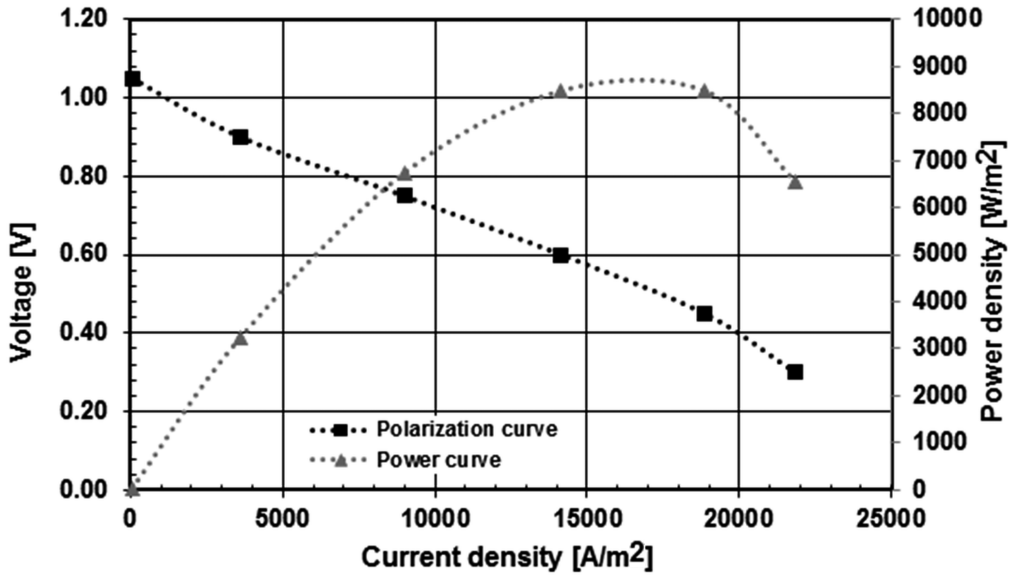

Fig. 4. PEMFC polarisation curve and power characteristic

Understanding water transport mechanism is crucial for prediction of PEMFC performance. Distributions of vapour mass fraction and liquid water at anode and cathode sides are shown in Fig. 5. It was confirmed that the vapour water content increased along the flow direction both at anode and cathode sides.

Furthermore, the greater operating voltage (i.e. the lower current), the bigger growth of water amount (0.37 kg/kg at 0.3 V and 0.46 kg/kg at 0.9 V at the outlet). The same trend existed in the case of liquid water. Moreover, the hydrogen and oxygen mass fractions and pressure, temperature distributions are displayed in Fig. 6. It was found that the mass fractions of oxygen and hydrogen were reduced along their flow direction. Additionally, the maximum utilisation of hydrogen was observed at the greatest voltage but the maximum utilisation of oxygen occurred at the lowest voltage. It was also noticed that the highest temperature occurred at the lowest voltage (and the greatest current).

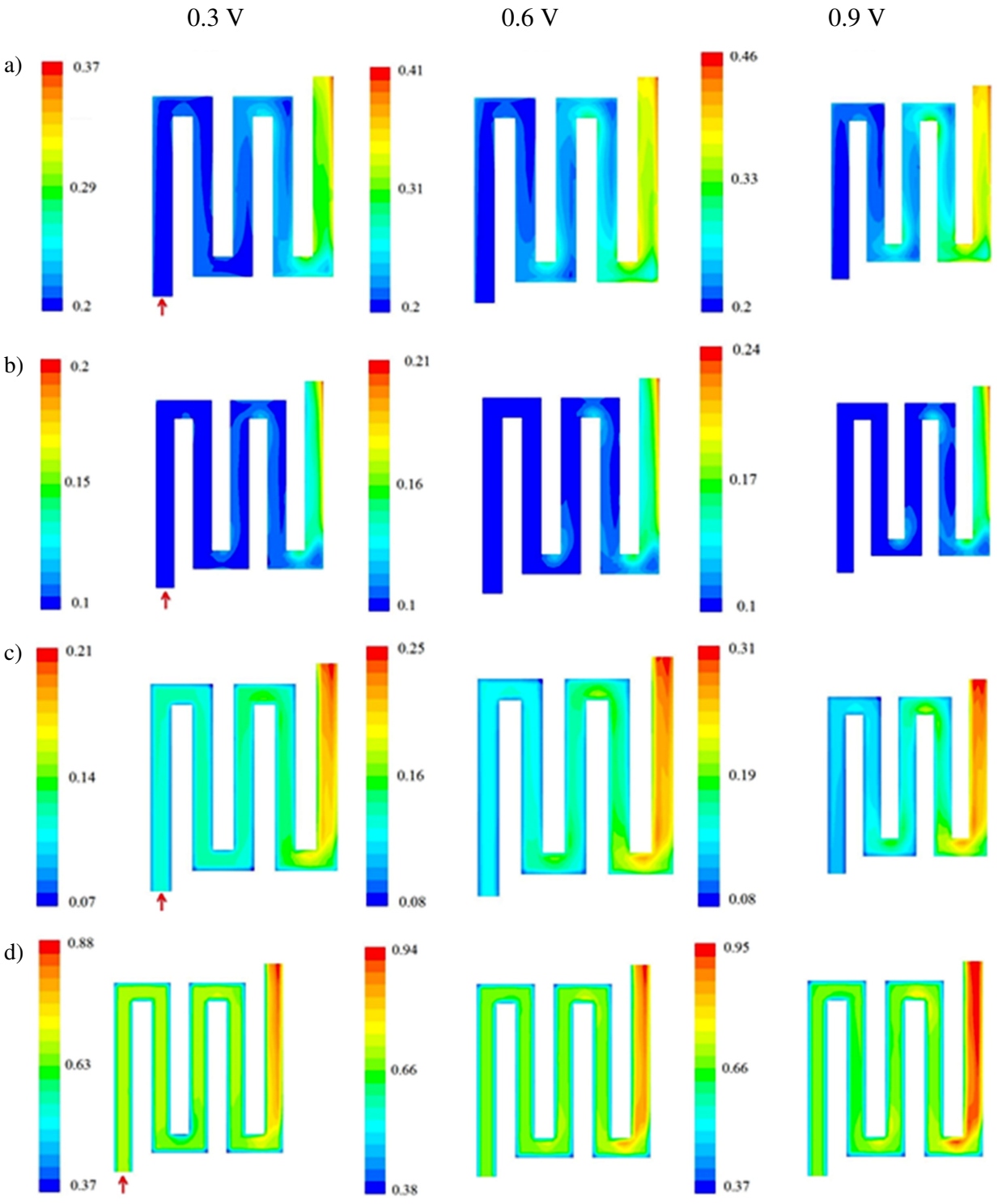

Fig. 5. Mass fraction [kg/kg] distributions of: a) vapour in anode, b) vapour in cathode, c) liquid water in anode, d) liquid water in cathode

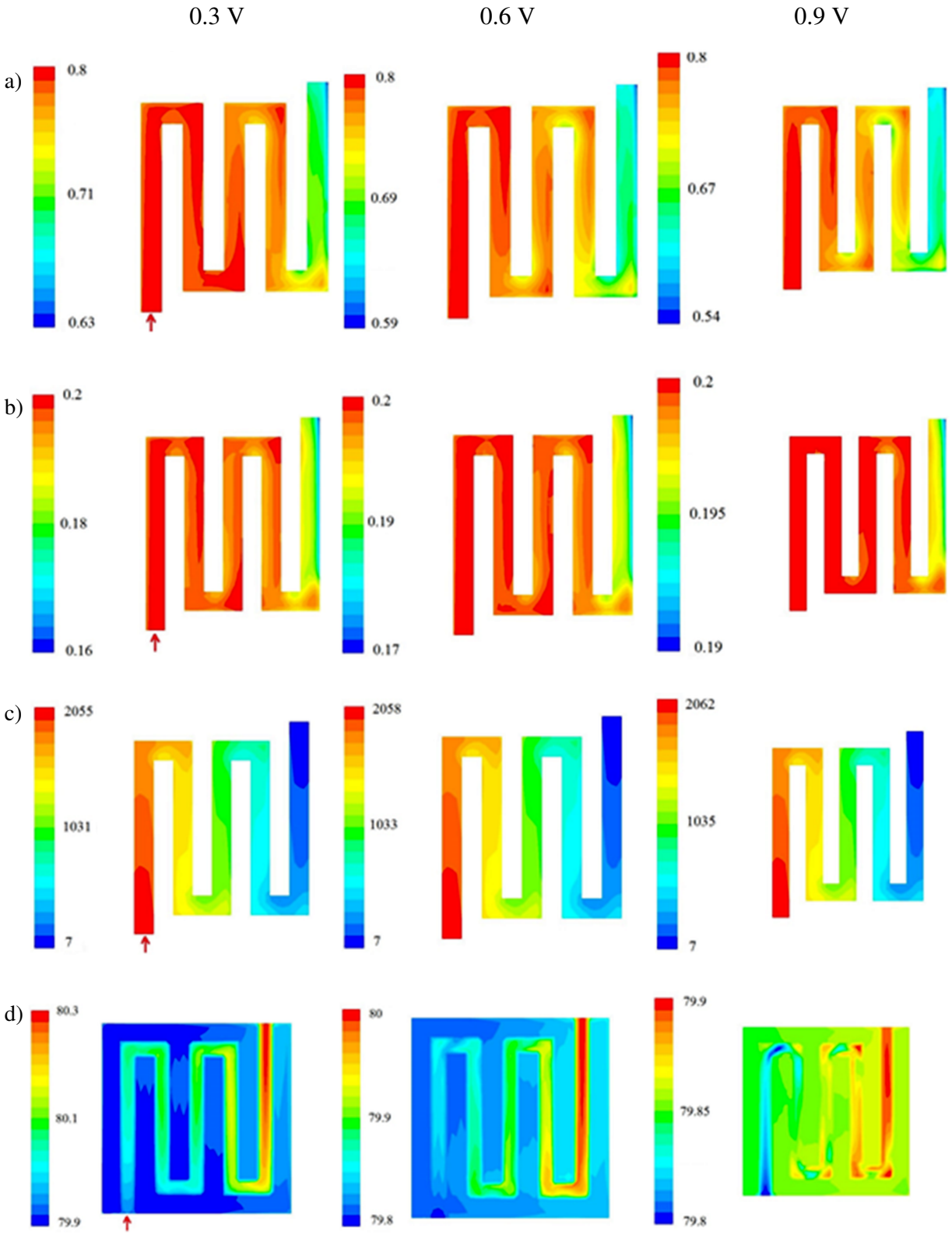

Fig. 6. Distributions of: a) mass fraction [kg/kg] of hydrogen, b) mass fraction [kg/kg] of oxygen, c) pressure [Pa], d) temperature [°C]

Finally, the current density distributions at membrane and terminal surface are indicated in Fig. 7. Different distributions of current density for various voltages at membrane surface can be seen. This was due to the fact that the PEMFC performance strongly depends on the mass, heat and charge transport. The region of the greatest current was noticeable at the outlet.

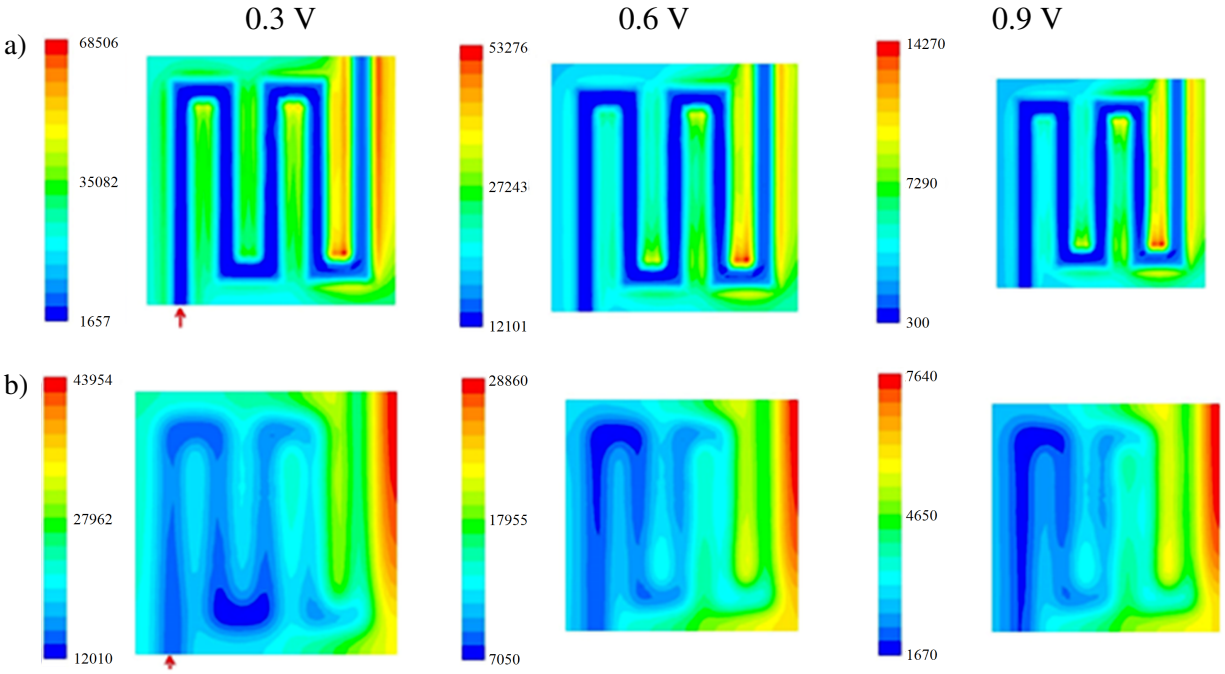

Fig. 7. Current density [A/m^2] distributions: (a) at membrane surface, (b) at terminal surface

4. CONCLUSIONS

In this study the calculated current – voltage curve and power characteristic in a wide scope of voltage for a novel design of Proton Exchange Membrane Fuel Cell with a serpentine micro-channel flow fields were obtained. This modelling allowed to reveal the extensive influence of flow fields and phenomena inside the fuel cell on the PEMFC performance. The effect of operating voltage on gas species, liquid water content and flow was studied. It was noticed that the current distribution was not uniform and depended on the flow design. The anode side of membrane was more susceptible to drying than the cathode one. It has been demonstrated that a proper water management plays a crucial role in the overall PEMFC performance as proton conductivity is directly proportional to the water content.

SYMBOLS

c_p	heat capacity, J/(kg·K)
D_j	diffusivity coefficient of species, m^2/s
F	Faraday constant, C/mol
h_{phase}	the latent heat of water term, J
h_{reaction}	the heat of formation of water term, J
I	current, A
j^{ref}	reference exchange current density, C/(m^2·s)
J	diffusive flux, 1/m^{2}s
K	permeability of layer, m^2
k	thermal conductivity, W/(m·K)
$M_{w,j}$	molecular mass of the respective species, kg/mol
n	number of electrons released in a reaction
p	pressure, Pa
R	gas constant, J/(K·mol)

R_{Ohm}	electric resistance, Ohm
$R_{s/m}$	volumetric transfer current, C/(m^2·s)
r	ratio of the specific reactive surface area to volume
r_s	exponent of pore blockage
s	volume fraction of liquid water (water saturation)
S	source term, mol/(m^3·s)
t	time, s
T	temperature, K
V_{OC}	open circuit voltage, V
X	local species concentration, mol/m^3
y	mass fraction of species, kg/kg

Greek symbols

α	transfer coefficient
β, ϖ	membrane conductivity coefficients
δ	average distance between the reaction surface and cell center, m
ε	porosity
λ	stoichiometry coefficient
μ	dynamic viscosity, Pa·s
η	activation loss, V
ρ	density, kg/m^3
$\bar{v}$	velocity vector, m/s
σ_s	electrical conductivity of solid zone, 1/(Ohm·m)
σ_m	membrane electrical conductivity, 1/(Ohm·m)
φ	electric potential, V

Subscripts

j	chemical species
s	solid phase
f	fluid phase
an/cat	anode/cathode
mem	membrane

The research program leading to these results was financed by the Polish research funds awarded for the project No. 517-10-013-5963/17.

REFERENCES

ANSYS Inc., 2015. *ANSYS Fluent Fuel Cell Modules Manual*.

Ferreira R.B., Falcão D.S., Oliveira V.B., Pinto A.M.R.F., 2017. 1D + 3D two-phase flow numerical model of a proton exchange membrane fuel cell. *Appl. Energy*, 203, 474–495. DOI: 10.1016/j.apenergy.2017.06.048.

Ju H., Wang C-Y., 2004. Experimental validation of a PEM fuel cell model by current distribution data. *J. Electrochem Soc.*, 151 (11), A1954–A1960. DOI: 10.1149/1.1805523.

Kahveci E.E., Taymaz I., 2018. Assessment of single-serpentine PEM fuel cell model developed by computational fluid dynamics. *Fuel*, 217, 51–58. DOI: 10.1016/j.fuel.2017.12.073.

Kunusch C., Puleston P., Mayosky M., 2012. *Sliding-mode control of PEM fuel cells*. *Advances in Industrial Control*. Springer-Verlag, London, 13–33. DOI: 10.1007/978-1-4471-2431-3.

Lafmejani S.S., Olesen A.C., Kær S.K., 2017. VOF modelling of gaseliquid flow in PEM water electrolysis cell micro-channels. *Int. J. Hydrogen Energy*, 42, 16333–16344. DOI: 10.1016/j.ijhydene.2017.05.079.

Li H., Knights S., Shi Z., Van Zee J.W., Zhang J., 2010. *Proton Exchange Membrane Fuel Cells: Contamination and mitigation strategies*. CRC Press, Boca Raton, 20–339.

Quan P., Zhou B., Sobiesiak A., Liu Z., 2005. Water behavior in serpentine micro-channel for proton exchange membrane fuel cell cathode. *J. Power Sources*, 152, 131–145. DOI: 10.1016/j.jpowsour.2005.02.075.

Springer T. E., Zawodzinski T.A., Gottesfeld S., 1991. Polymer electrolyte fuel cell model. *J. Electrochem Soc.*, 138, 2334–2342. DOI: 10.1149/1.2085971.

Taner T., 2018. Energy and exergy analyze of PEM fuel cell: a case study of modeling and simulations. *Energy*, 143, 284–294. DOI: 10.1016/j.energy.2017.10.102.

Vega-Leal A.P., Palomo F.R., Barragán F., García C., Brey J.J., 2007. Design of control systems for portable PEM fuel cells. *J. Power Sources*, 169, 194–197. DOI: 10.1016/j.jpowsour.2007.01.055.

Wang X-D., Duan Y-Y., Yan W-M., Lee D-J., Su A., Chi P-H., 2009. Channel aspect ratio effect for serpentine proton exchange membrane fuel cell: Role of sub-rib convection. *J. Power Sources*, 193, 684–690. DOI: 10.1016/j.jpowsour.2009.04.019.

Yue L., Wang Y., Wang S., 2017. New design of a cathode flow-field with a sub-channel to improve the polymer electrolyte membrane fuel cell performance. *J. Power Sources*, 344, 32–38. DOI: 10.1016/j.jpowsour.2017.01.075.

Received 21 September 2017
Received in revised form 20 April 2018
Accepted 20 April 2018